INT. J. NUM. METH. HEAT FLUID FLOW, VOL. 3, 399–410 (1993)

VORTEX INITIATION DURING DYNAMIC STALL OF AN AIRFOIL

I. P. ITTY AND J. R. LEITH

Department of Mechanical Engineering, The University of New Mexico, Albuquerque, NM 87131, USA

ABSTRACT

The flow field around an oscillating airfoil is evaluated numerically, using the stream function–vorticity formulation of the Navier–Stokes equations. An algebraic turbulence model, adapted from the Baldwin–Lomax model, is included in solving the time-averaged Reynolds equations. Computed pressure distribution for turbulent flow past a stationary airfoil is compared with measurements. Finally, for the oscillating airfoil cases, the computations are performed in order to determine the history of pressure distribution and to identify the nature of the vortex initiation on the suction surface for laminar and turbulent flow. Our results for laminar flow show that minute circular shaped vortices are formed on the surface prior to the dominant vortex formation. Flattened vortices are formed on the surface in turbulent flow, prior to the formation of the dominant large vortex structure.

KEY WORDS Vortex initiation Dynamic stall Turbulence modelling Inertial reference frame

INTRODUCTION

Numerical solution to the Navier–Stokes equations is usually based upon primitive variable form, velocity–vorticity form or stream function–vorticity form. Many researchers have used the primitive variable form of the compressible Navier–Stokes equations for analysing high Reynolds number flows, making use of either the Beam and Warming approximate factorization scheme[1] or its variations[2,3]. It is known that the unsteady compressible Navier–Stokes equations are a mixed set of hyperbolic(space)–parabolic(time) equations, while the unsteady incompressible Navier–Stokes equations are a mixed set of elliptic(space)–parabolic(time) equations. As a consequence, the solution methods for the incompressible Navier–Stokes equations involve iterations at every time step, unlike the methods for the compressible form of the equations. The compressible and incompressible forms of the equations are solved using different numerical techniques. A zonal method was used by Wu *et al.*[4] for solving the velocity–vorticity form of the equations. Boisson *et al.*[5] have numerically predicted low Reynolds number turbulent flow around a cylinder using the velocity–vorticity form. Daube *et al.*[6] simulated laminar flow around an oscillating airfoil employing the stream function–vorticity form of the Navier–Stokes equations for $Re = 3000$.

Mehta[7] developed an algorithm to analyse laminar external flows up to $Re = 10^4$, which used the stream function–vorticity formulation. This paper describes the modifications of Mehta's algorithm to predict high Reynolds number incompressible turbulent flows. The Reynolds time-averaged vorticity transport equation and the stream function equation are solved. An analysis of the computed Navier–Stokes solution, emphasizing the vortex initiation on the surface of an oscillating airfoil and the time history of pressure distribution, is the subject matter of this paper.

0961–5539/93/050399–12$2.00

Received December 1991
Revised September 1992

The calculated pressure distribution for steady flow past a NACA 0012 airfoil is compared with measurements. Next, the velocity distribution in the near wake for the oscillating case under stall limit is considered for quantitative comparison. Finally, laminar and turbulent flow fields around an airfoil, which oscillates in the stall regime, are investigated. The computed results are compared qualitatively with available experimental results and the phenomenon of dynamic stall is studied to identify the stages and to distinguish vortex initiation.

MATHEMATICAL MODEL

For incompressible, unsteady flow with constant molecular viscosity and in the absence of body forces, a non-dimensional coordinate invariant form of the time-averaged Reynolds equation is given by[9]:

the total derivative of velocity:

$$\frac{DV}{Dt} = \nabla\tau \tag{1}$$

where

$$\tau = [-p]\mathbf{I} + \frac{L}{Re}(1 + v_N)[\nabla\mathbf{V} + (\nabla\mathbf{V})_c] \tag{2}$$

Here, v_N is the ratio of kinematic eddy viscosity to kinematic molecular viscosity. The other notations are: Re, Reynolds number, p, pressure, V, velocity vector and I, identity tensor. Also, note that $((\nabla\mathbf{V} + (\nabla\mathbf{V})_c)/2)$ represents the symmetric rate of strain dyadic. The free stream velocity U_∞ and the radius of the circle, a, associated with the grid transformation are the characteristic velocity and length scales respectively. The characteristic time is chosen, as in Reference 7, such that time $t' = t(a/U_\infty)$.

If the coordinate system is fixed with respect to the airfoil which is rotating with an angular velocity Ω relative to the inertial system, the velocity V relative to the non-Newtonian reference frame (NNRF) of a point located by the vector r is given by,

$$\mathbf{V}_I = V + \Omega \times \mathbf{r} \tag{3}$$

The angular velocity is defined as positive in the counter-clockwise direction. The coordinate system is illustrated in *Figure 1*. The axes OX–OY form the NNRF, and OX_I–OY_I form the inertial reference frame. In the current iuvestigations, the direction OX is the chordwise direction and OY is the pitchwise direction. Also, the axis OX is referred to as the centreline. The distances x and y, are measured along OX and normal direction OY respectively. For positive values of α, the region above the centreline is considered as the suction region and below it as the pressure region.

The governing equation with respect to the NNRF notation is:

$$\frac{D\mathbf{V}}{Dt} + \frac{d\Omega}{dt} \times \mathbf{r} + 2\Omega \times \mathbf{V} + \Omega \times (\Omega \times \mathbf{r}) = \nabla\cdot\tau \tag{4}$$

Here, the first term represents the sum of local and convective acceleration. The next three terms correspond to Eulers acceleration, Coriolis acceleration and centrifugal acceleration respectively. The right hand side represents the normal force and shear force created in the flow per unit mass.

Now define vorticity: $\omega = \nabla \times \mathbf{V}$ and the stream function by equating $\mathbf{V} = \nabla \times \psi$ where $\psi = (0, 0, \psi)$. The vorticity transport equation based on Boussinesq hypothesis for Reynolds stresses is obtained by taking the curl of (4). Note that the Coriolis and centrifugal forces vanish in the transformation.

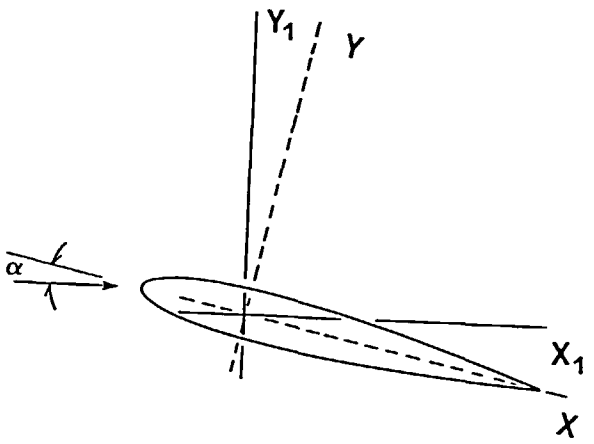

Figure 1 Coordinate reference frames

The time-averaged vorticity equation is obtained by considering the curl of (4) as:

$$\frac{\partial(\omega + 2\Omega)}{\partial t} - \nabla \times (\mathbf{V} \times \omega) = \frac{L}{Re}\nabla^2(1 + \nu_N)\omega + \mathrm{S}_\omega \tag{5}$$

where S_ω is comprised of elements referred to as source terms by Gosman *et al.*[10] and for two-dimensional flow, the vorticity vector, $\omega = (0, 0, \omega)$. The source terms in the cartesian coordinates for two dimensional flow is given by[11,12]:

$$2\frac{L}{Re}\left[\frac{\partial^2}{\partial x^2}\left(\nu_N\frac{\partial u}{\partial y}\right) - \frac{\partial^2}{\partial y^2}\left(\nu_N\frac{\partial v}{\partial x}\right) + \frac{\partial^2}{\partial x\partial y}\left(\nu_N\frac{\partial v}{\partial y}\right) + \frac{\partial^2}{\partial x\partial y}\left(\nu_N\frac{\partial u}{\partial x}\right)\right]$$

The source terms in (5) contain both second-order derivative terms in vorticity and fourth-order derivative terms in stream function and they are proven to be negligible[11,12].

Hence for the present computations, the time-averaged vorticity transport equation of the form,

$$\frac{\partial(\omega + 2\Omega)}{\partial t} - \nabla \times (\mathbf{V} \times \omega) = \frac{L}{Re}\nabla^2(1 + \nu_N)\omega \tag{6}$$

and the stream function equation:

$$\nabla \times \mathbf{V} = \omega \tag{7}$$

are solved.

The coordiuate transformation maps the field exterior to the body into a unit circle. The vorticity transport equation (6) in the Joukowski plane $(r - \theta)$ is:

$$H^2r^2\frac{Re}{L}\frac{\partial(\omega + 2\Omega)}{\partial t} = \nabla^2(\nu_N + 1)\omega - r\frac{Re}{L}\left\{\frac{\partial\omega}{\partial r}\frac{\partial\psi}{\partial\theta} - \frac{\partial\omega}{\partial\theta}\frac{\partial\psi}{\partial r}\right\} \tag{8}$$

and the stream function ψ is defined by the equation:

$$\nabla^2\psi = -H^2r^2\omega \tag{9}$$

in which rH^2 is the Jacobian of the coordinate transformation from the physical to Joukowski planes $(x, y) \rightarrow (r, \theta)$.

Factorization scheme

The philosophy adopted in the numerical scheme is to let the governing equation and the non-slip surface boundary condition dictate the flow field with a weak condition at the outer boundary. The exact factorizing scheme applied to the vorticity transport equation, taking into account the Reynolds stress terms, is described below. Equation (8) in the ρ–θ plane is:

$$H^2r^2\frac{Re}{L}\frac{D\omega_I}{Dt}=\left[\left(r\frac{\partial\rho}{\partial r}\right)^2\frac{\partial^2}{\partial\rho^2}+\left(r\frac{\partial\rho}{\partial r}+r^2\frac{\mathrm{d}^2\rho}{\mathrm{d}r^2}\right)\frac{\partial}{\partial\rho}+\frac{\partial^2}{\partial\theta^2}\right](\omega_1+v_N\omega_I) \tag{10}$$

where $\omega_I=\omega+2\Omega$. Now, by defining $A=H^2r^2(Re/L)$ and the differential operators

$$\partial_\rho^n=\left[\left\{\left(r\frac{\mathrm{d}\rho}{\mathrm{d}r}\right)^2\frac{\partial^2}{\partial\rho^2}+\left(r\frac{\mathrm{d}\rho}{\mathrm{d}r}+r^2\frac{\mathrm{d}^2\rho}{\mathrm{d}r^2}\right)\frac{\partial}{\partial\rho}\right\}(1+v_N)-r\frac{\mathrm{d}\rho}{\mathrm{d}r}\frac{Re}{L}\frac{\partial}{\partial\rho}\frac{\partial\psi}{\partial\theta}\right]$$

and

$$\partial_\theta^n=\left[\frac{\partial^2}{\partial\theta^2}(1+v_N)+r\frac{\mathrm{d}\rho}{\mathrm{d}r}\frac{Re}{L}\frac{\partial}{\partial\theta}\frac{\partial\psi}{\partial\rho}\right]$$

neglecting the subscript I for brevity, (3) reduces to the form:

$$A\frac{\partial\omega}{\partial t}=\partial_\rho^n\omega+\partial_\theta^n\omega \tag{11}$$

Using a three point backward differencing in time, (11) is:

$$A\left(\frac{T_3\omega^{n-2}+T_2\omega^{n-1}+T_1\omega^n}{2\Delta t}\right)=(\partial_\rho^n+\partial_\theta^n)\omega^n \tag{12}$$

The three point backward differencing is formulated by choosing $T_1=3$, $T_2=-4$, and $T_3=1$; while the two point scheme is formulated by setting $T_1=2$, $T_2=-2$ and $T_3=0$. The order of differencing in time, $m=2$ for three point differencing, and $m=1$, for two point differencing. Whenever the time step during the computation is halved, $m=1$ for that particular time step.

The factorized form of the above equation is:

$$\left(1-\frac{2\Delta t}{AT_1}\partial_\theta^n\right)\bar{\omega}=-\frac{1}{T_1}(T_3\omega^{n-2}+T_2\omega^{n-1})+4\frac{\Delta t^2}{T_1^2A^2}\partial_\theta^n\partial_\rho^n\omega$$

$$\left[1-\frac{2\Delta t}{AT_1}\partial_\rho^n\right]\omega=\bar{\omega} \tag{13}$$

The above equations are the exact factorized form of the vorticity transport equation. The approximate factorization scheme[1] or its variations[2,3] either neglect the cross derivative terms or lag the evaluation of these terms by one time step. Both these operations will reduce the time accuracy.

The derivatives with respect to θ are replaced by fourth-order accurate rational fractions utilizing a fast Fourier transform algorithm, and the derivatives in the ρ direction are approximated by second order differences. The fourth-order accurate form of differencing is stated as follows:

$$\frac{\partial f}{\partial\theta}=\frac{D_0f}{1+\dfrac{\Delta\theta^2}{6}D_+D_-} \tag{14}$$

$$\frac{\partial^2 f}{\partial\theta^2}=\frac{D_+D_-f}{1+\dfrac{\Delta\theta^2}{12}D_+D_-}$$

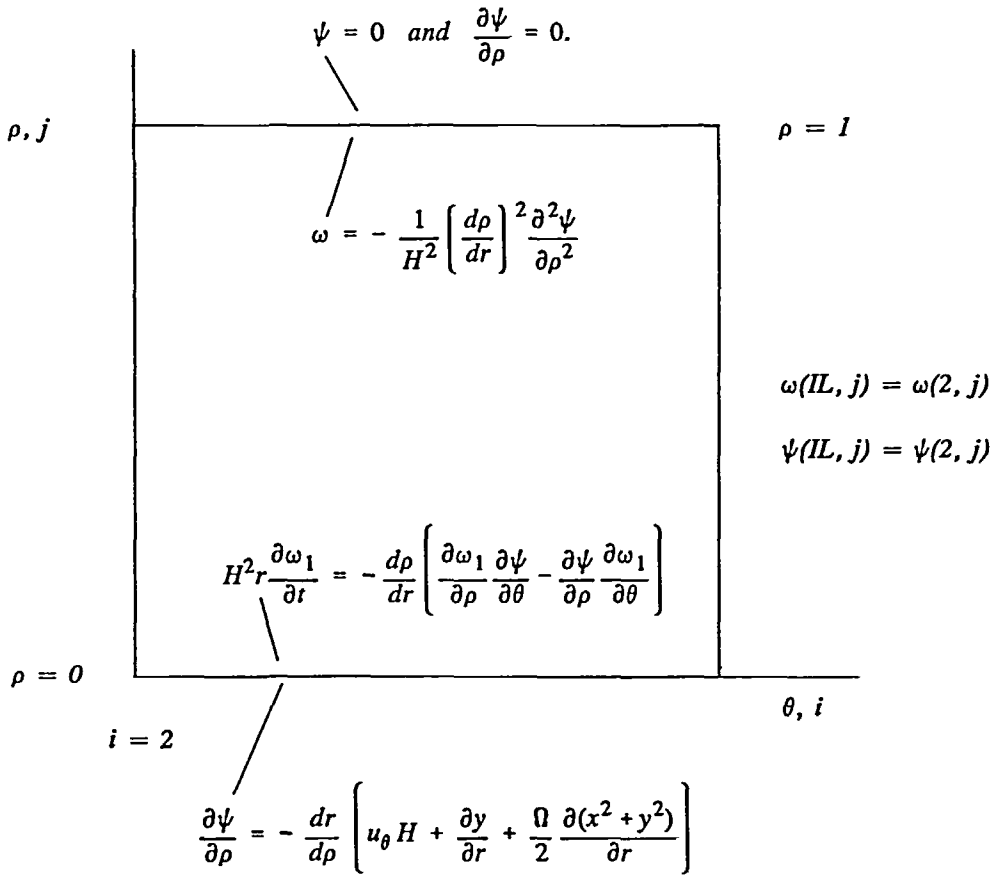

Figure 2 Boundary conditions in the transformed plane

$$D_0 f = \frac{f_{i+1} - f_{i-1}}{2\Delta\theta} \tag{15}$$

and

$$D_+ D_- f = \frac{f_{i+1} - 2f_i + f_{i-1}}{\Delta\theta^2} \tag{16}$$

The stream function equation is solved using the fast Fourier transform technique coupled with the Pade differencing[7,8]. The Fourier transform of the stream function equation in the computational plane ρ–θ is solved. The surface vorticity is evaluated using the second-order accurate Woods formulation[7]. The outer boundary condition is such that the inertia force is predominant, and at the surface, no-slip boundary condition is enforced as shown in *Figure 2*.

We improved the algorithm in Reference 7 to predict high Reynolds number flows as follows. In order to solve the above-mentioned factorized form of the vorticity transport equation and the stream function equation for every time step, the stream function and vorticity values are predicted from previous time levels, at the beginning of the intra-time step iteration[7]. Always the interior values of vorticity and stream function are chosen to be the most recent values in calculating the Reynolds stresses. Then, the surface vorticity is evaluated ensuring the no-slip

boundary condition. The surface vorticity is then underrelaxed at every time step n as follows, until convergence is attained:

$$\omega_{\text{wall}}^{n,s} = \omega_{\text{wall}}^{n,s-1} + \beta(\omega_{\text{wall}}^{n} - \omega_{\text{wall}}^{n,s-1}) \tag{17}$$

where s is the iteration index and n is the time-step. The computational scheme is sensitive to the choice of the relaxation parameter β, and we propose the choice of this parameter as follows:

$$\beta = \lambda H^{2m} \tag{18}$$

It can be observed that, since H is a scale factor, (18) is a generalized equation in which the parameter β is a smooth function of the fineness of the grid distribution on the surface. The constants λ and m are varied independently for the minimum number of iterations for convergence to a prescribed change in vorticity on the surface. These constants depend on the free stream Reynolds number and the profile of the body. Although the values of the relaxation parameter are not unique, the form of (18) relating the relaxation parameter to the Jacobian is the interesting feature of the formula. The computational grid arrangement is comprised of 128 grid points in the azimuthal direction and 96 grid points in the pseudo-radial direction. The time step Δt is chosen as constant. The residue $(= (\omega_{\text{wall}}^{s} - \omega_{\text{wall}}^{s-1})/\omega_{\text{wall}}^{s})$ on the evaluation of surface vorticity between successive iterations at every time step was 2×10^{-4} in most of the computations. Dependent on the size of time step and the strength of vorticity change, the number of iterations for convergence of the surface vorticity varied from 2 to 12.

Despite great progress in turbulence research, the use of higher equation models for a problem of this kind does not appear to merit the computational effort to date. This can be attributed to the unavailability of the transport constants, damping functions and the nature of wall function for massively separated flows. It is known that an algebraic turbulence model, without the requirement to evaluate the boundary layer thickness, is suitable for Navier–Stokes codes[4,13]. Hence the model due to Baldwin and Lomax has been used[13]. The model has been modified to the non-dimensional form suitable for the present formulation. The Baldwin–Lomax model is used in attached and separated flow regions as well as in wakes. There exist a fair amount of discrepancies[13] in determining the most relevant peak in the vorticity function $F = Dy\omega$, where D is the damping function. In the present calculation, the peak is confined to the outer layer of the boundary layer by choosing the value in the neighbourhood of the region where $(\omega/\omega_{\text{wall}}) < 0.002$. After the separation point, the nearest peak to the wall is chosen to capture the effects of the secondary vortices[13], for the analysis of flow around a cylinder. The inner layer has been modified for free turbulence effects in the near wake. A variation of the algebraic model proposed by Cebeci *et al.*[14] has been used to accomplish this (see Reference 7 for details).

RESULTS AND DISCUSSION

Preliminary investigations

We have evaluated steady-state solution for flow past a NACA 0012 airfoil at $Re = 760{,}000$, as experimental data are available at this Reynolds number[15]. Pressure distribution on the surface has been obtained by integrating the tangential component of momentum equation (1) on the surface, using a fourth-order accurate difference scheme. The tangential component of (1) on the surface can be written as:

$$\frac{\mathrm{d}p}{\mathrm{d}\theta} = \frac{L}{Re}\frac{\mathrm{d}}{\mathrm{d}r}((1 + \nu_N)\omega)|_{\text{wall}} \tag{19}$$

The agreement with the pressure distribution improved significantly, as explained later, by using second-order accurate one-sided differences for the transverse gradient of vorticity in (19). This

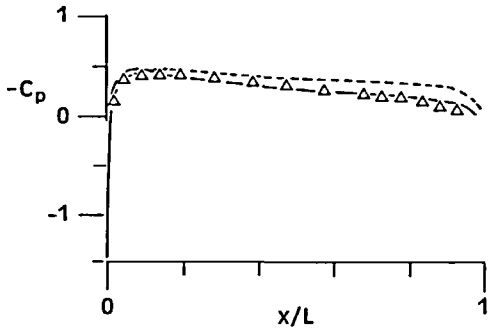

Figure 3 Pressure distribution on NACA 0012 airfoil, $Re = 7.6 \times 10^5$. Δ, experimental[15]; ——, first-order differences; ———, second-order differences[8] for $(d(1 + \nu_N)\omega)/dr)_{wall}$ in (19)

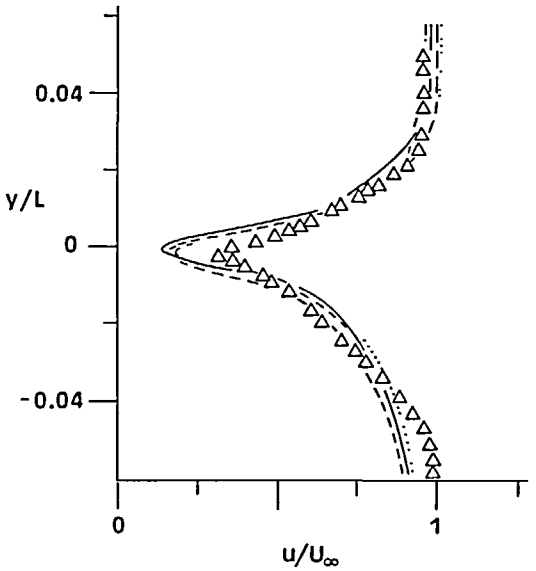

Figure 4 Chordwise velocity distribution in the near wake, $\alpha = 0°$. Δ, experimental[16]; ———, present method; —, cycle 1; –, cycle 2; · · · ·, cycle 3; –·–, cycle 4. $Re = 3 \times 10^5$, $\alpha = 5 - 5\cos(ft)$, $k = 1.01$, $x/L = 1.007$

improvement for laminar flow has been reported by Roache & Salari[3] by comparing the results of the present code with that of a compressible Navier–Stokes code for flow past a NACA 0012 airfoil at $Re = 5000$. *Figure 3* shows the comparison of pressure coefficient[8] with experimental results for fully turbulent flow. Further, the comparison illustrates that the pressure distribution on the surface is dependent on the distribution of eddy viscosity in the normal direction. Thus, determination of the pressure coefficient using surface pressure quadrature expressions can serve as a check for the distribution of eddy viscosity near the wall.

Next, an oscillating airfoil case under the stall regime is considered for quantitative comparison with available experimental results[16] in *Figure 4*. It may be noted that the results of numerical computations and experiments vary from one cycle of oscillation to another[13,16,19]. The airfoil completes one cycle of oscillation, as the flow traverses through approximately three times the chord distance.

There are 16 grid points at $x/L = 1.007$ and 10 points at $x/L = 1.02$, within $-0.05 < y/L < 0.05$. The computed velocity profiles are smoothed by using a parametric fifth-order polynomial and are shown in Reference 8. *Figure 4* presents the variation of chordwise velocity in the transverse direction at $x/L = 1.007$ for four successive cycles when the instantaneous angle of attack is zero. The scatter in the computed results for a particular angle of attack during the four cycles of oscillation is identified. Hence comparison of computed results with experimental results must be made with caution. The experimental results[16,18] and the results of numerical calculations from one cycle of oscillation to another vary, despite the externally controlled variables remain the same. The reasons for this unavoidable variation of the results within the context of experiments and numerical computations differ from each other. The likely causes include inhomogeneous medium, wind tunnel effects, vibration and human factors. In a computational environment, the scatter of results occur as a result of truncation error, inadequate grid resolution, inaccurate far field boundary conditions, inability to model the turbulence correctly and the limited domain of computation (6 times the chord distance

here). Experimentalists usually represent the results as an average over a series of cycles, ranging from 50 to 250, depending on the severity of the case under study[16,19].

However, numerical experiments do not seem to proceed up to this many cycles because of the high cost of computation. In addition to this, it may be worthwhile to note the purpose of computational fluid dynamics which is to bring physical insight into fluid mechanics problems, that are not forthcoming from experiments[17], rather than duplicating experimental results.

With these in mind the following is a qualitative study of dynamic stall to identify the stages, and to distinguish vortex initiation between laminar and turbulent flow cases.

Flow field around an oscillating airfoil under stalled conditions

We have computed a laminar flow case for an oscillating NACA 0012 airfoil at a Reynolds number of 21,000. For this case, the angle of attack is given by $\alpha = 10 - 10\cos(ft)$ and the reduced frequency, k, is $= (fl/2U_\infty) = 0.25$. Here, f is the circular frequency of oscillation, t is the non-dimensional time since the resumption of oscillation and l is the chord length. In the non-dimensional sense, the airfoil has to traverse through twelve times the chord distance approximately for a complete cycle of oscillation. The flow parameters have been chosen to compare results with the experimental results presented by McAlister *et al.*[18]. This case corresponds to a turbulent near wake and laminar flow field around the airfoil. Although McAlister *et al.* have reported the history of the flow behaviour, based on their flow visualization experiments, this paper attempts to explain the behaviour based on the pressure distribution, computed streamlines and vorticity contours. The details of the complete flow behaviour for a complete cycle of oscillation are represented in Reference 8.

Figure 5 illustrates the vortex formation stage during the pitch-up motion of the airfoil, in terms of flow visualization diagrams coupled with the computed streamlines and vorticity contours. It is noted that the actual flow visualization diagrams neither represent the streamlines nor the vorticity contours. That is, the flow visualization results in *Figure 5* are the trajectories of hydrogen bubbles and can be considered as representative of the viscous regions[18].

History of surface pressure

Pressure distribution on the surface can often be determined from experiments and it represents the normal stress on the surface. Hence, various researchers have used the surface pressure distribution in order to identify the flow characteristics. The variation of pressure coefficient on the upper surface of the airfoil as a function of chord distance and the angle of attack is depicted in *Figure 6*. The effect of the initiation growth and shedding of the vortex can be analysed by comparing the pressure distribution to the structure of the flow field illustrated in terms of streamlines and vorticity contours[8]. The leading edge pressure (suction) peak at $\alpha = 17.1$ degrees gives an indication that the dynamic stall has begun. That is, the formation of the stall vortex near the leading edge, although small in size, creates the sharp gradient in pressure coefficient illustrated in *Figure 6*. The simulations show[8] that a vortex structure forms near the trailing edge as α is increased, and this structure eventually merges with the leading edge vortex to form the dominant vortex structure on the upper surface. As α increases further, this vortex grows in size as it moves downstream on the airfoil. At about $\alpha = 19.7°$ a secondary vortex forms near the leading edge. The dip in the pressure distribution (*Figure 6*) is apparently caused due to this sequence of events. As soon as the pitching motion reverses in direction the clockwise vortex initiated at the leading edge grows in size considerably, and leaves the surface at about three-quarters of the chord distance from the leading edge (α reduces from 18.7 to 17.1°). In the meantime, a third vortex is formed around the quarter-chord location. This vortex grows to a lesser size than its predecessor and travels on the surface of the airfoil and leaves to the near wake from the trailing edge ($\alpha = 10°, t = 84.9$). Following this vortex, the fourth vortex is formed and leaves the surface from the trailing edge. However, it can be observed that the size and

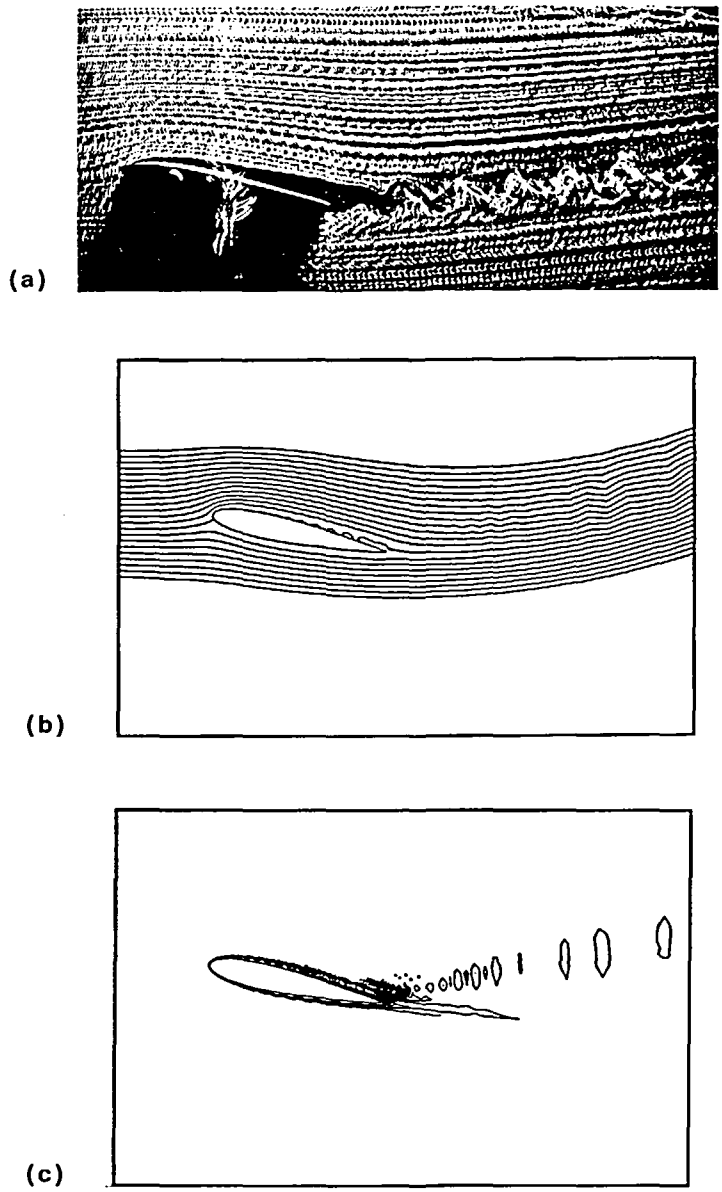

Figure 5 Flow characteristics around an oscillating airfoil, $\alpha = 10°$, pitching up, $Re = 2.1 \times 10^4$, $k = 0.25$; $t = 0.62$. (a) Flow visualization, hydrogen bubbles in water[18]; (b) computed streamlines; (c) vorticity contours

intensity of the vortices reduce, as the angle of attack approaches zero, during the pitch-down motion. This sequence of events during a complete cycle of oscillation can be divided into three different stages; movement of suction peak towards the leading edge with increasing magnitude (0–17.1°, stage 1); creation of multiple peaks of reduced magnitude and their movement towards the trailing edge (17.1–18.7° pitch-down, stage 2) and the flattening of the pressure distribution during the rest of the cycle (stage 3). The lift coefficient fluctuates from -0.5 to 2.5. The vortex formation and its shedding can be inferred from this diagram. During the pitch up motion of

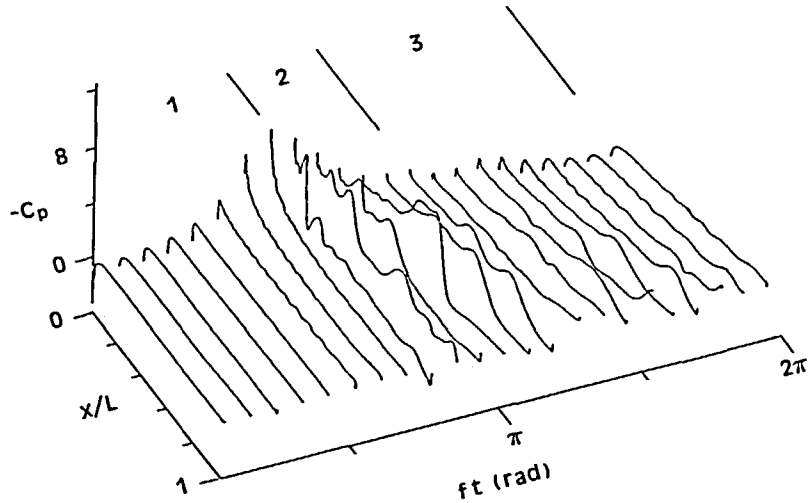

Figure 6 Temporal variation of C_p on the upper surface of a pitching airfoil, $\alpha = 10 - 10\cos(ft)$

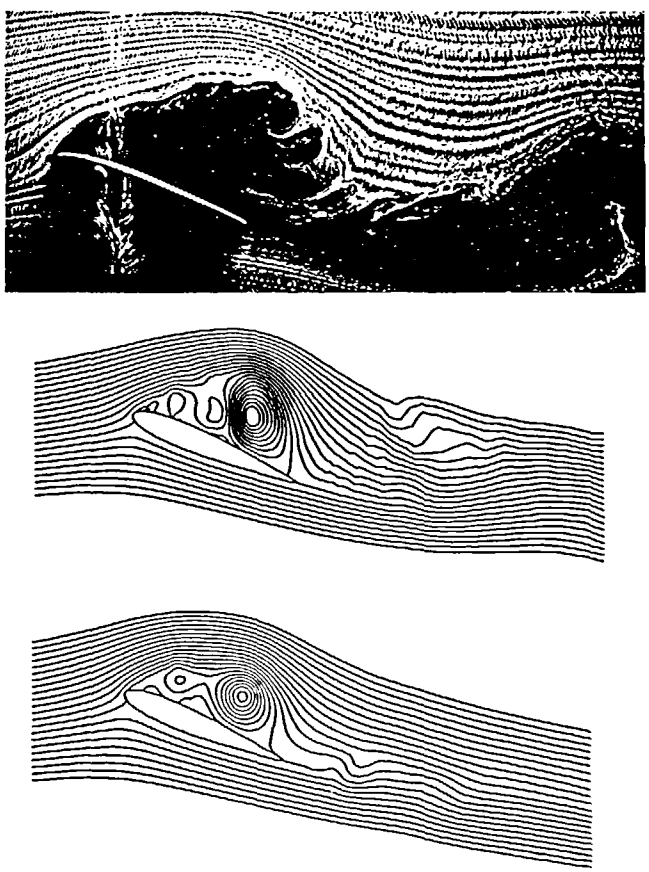

Figure 7 Comparison of streamline pattern between two successive cycles, $\alpha = 18.7°$, pitching down. $\alpha = 10 - 10\cos(ft)$

the airfoil the shedding of the leading edge vortex causes an increase in lift before the maximum angle of attack is reached. The maximum drag coefficient (= 0.73) occurs at the beginning of the downward motion. This behaviour is observed by McCroskey *et al.*[19] during their experiments.

The variation of the streamline pattern for the same incidence between successive cycles is shown in *Figure 7*. An estimate of variation of the results from cycle to cycle is in order. The scatter of the results from cycle to cycle is quoted by Lomax and Mehta[13], by comparing computed results with measurements, averaged over a series of cycles. McAlister *et al.*[18] have stated that the main events in the flow field vary by 2 degrees from cycle to cycle.

Effect of turbulence on the vortex initiation

We have computed a turbulent flow case for an oscillating NACA 0012 airfoil at a Reynolds number of 1×10^6, as illustrated in *Figure 8*. The behaviour of the streamline representing the surface reveals valuable information regarding the bubble formation on the suction surface during the pitch-up motion. A comparison of the turbulent case with the laminar case, reveals the following. In the laminar flow case, numerous small vortices are formed on the suction surface prior to the dominant vortex formation (see discussion above), whereas for the turbulent flow case, these initial vortices on the surface are more flat and less numerous. These minute vortices in turbulent flow reduce in size towards the leading edge, and are formed by the upward movement of the separation point as well as the effect from the curvature of the near wake. The vorticity contours[2] also illustrate the above-mentioned type of vortex initiation.

CONCLUSIONS

An improved relaxation parameter is utilized to predict high Reynolds number laminar and turbulent external flows around two-dimensional bodies. The vorticity–stream function formulation is used to analyse these external flows of engineering interest. Comparison of the computed results using algebraic turbulence models, with experimental results, is very favourable. It is well known that comparison of local skin friction coefficient is a reasonable criterion to check the turbulence model on the surface, as it represents the non-dimensional shear stress at the wall. The present analysis demonstrates that the comparison of pressure distribution on the surface also serves as an index to check the validity of the turbulence model in the region away from the surface.

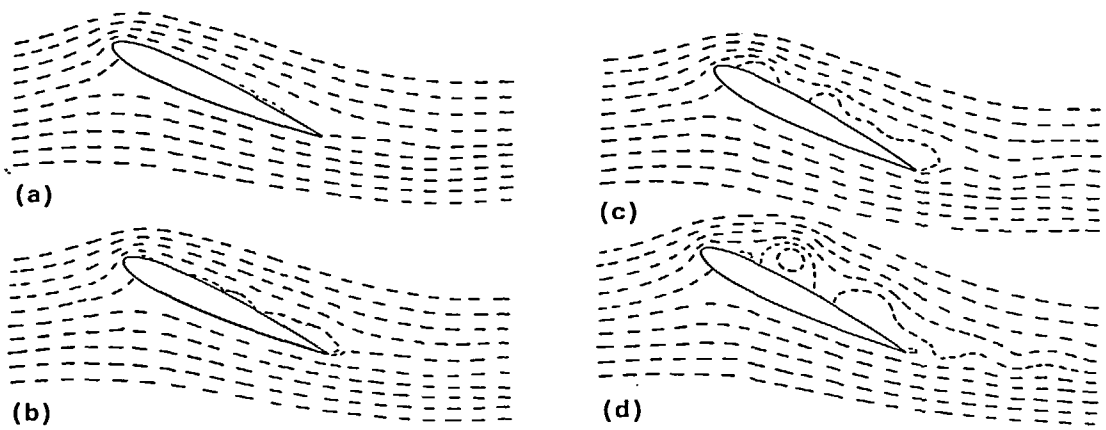

Figure 8 Streamline patterns demonstrating vortex initiation under fully turbulent flow conditions, $Re = 1 \times 10^6$, $\alpha = 15\text{–}14\cos(ft)$; $k = 0.1$, $\alpha =$ (a) 23.7°, (b) 24.83°, (c) 25.87°, (d) 26.78°

The paper identifies the three different stages in the pressure distribution, characteristic of dynamic stall on oscillating airfoils. It is possible to classify different cases of oscillation based on these stages. This information would aid in classifying the dynamic stall cases.

In the case of oscillation with stall, circular minute vortices on the surface precede the formation of the dominant vortex for the laminar case. For the turbulent case, however, several flat-shaped vortices are formed on the surface prior to the appearance of the dominant vortex. Usually aerodynamic design would aim at delaying the onset of stall for superior airfoil performance. Our results from supercomputer simulations are qualitatively consistent with previous experimental and numerical results reported in the literature. Where quantitative results are available, the presently reported simulations appear to predict the observed behaviour within the experimental errors realized.

ACKNOWLEDGEMENTS

The authors would like to thank Dr U. B. Mehta of NASA–Ames Research Center for providing the baseline algorithm and for many useful discussions. We also gratefully acknowledge the support from the National Center for Supercomputing Applications, University of Illinois. This work was partially supported by Air Force Contract No. F29601-85-C-0038.

REFERENCES

1 Beam, R. M. and Warming, R. F. An implicit factored scheme for the compressible Navier–Stokes equations, *AIAA Paper No. 77-645* (1977)
2 Tassa, Y. and Sankar, N. L. Dynamic stall of an oscillating airfoil in turbulent flow using time dependent Navier–Stokes solver, *Unsteady Turbulent Shear Flows* (Eds Michael, R., Cousteix, J. and Houdeville, R) Springer-Verlag, New York, p. 207 (1981)
3 Roache, P. J. and Salari, K. Weakly compressible Navier–Stokes solutions with an implicit approximate factorization code, *AIAA Paper No. 90-0235* (1990)
4 Wu, J. C., Wang, C. M. and Tuncer, I. H. Unsteady aerodynamics of rapidly pitched airfoils, *AIAA Paper No. 86-1105* (1986)
5 Boisson, H. C., Chassaing, P., Ha Minh, H. and Sevrain, A. Some characteristics of the unsteady wake flow past a circular cylinder, *Unsteady Turbulent Shear Flows* (Eds Michael, R., Cousteix, J. and Houdeville, R.) Springer-Verlag, New York, pp. 262–272 (1981)
6 Daube, O., Taphouc, L., Dalieu, A., Coutance, M., Ohmi, K. and Texier, A. Numerical solution hydrodynamics visualisation transient viscous flow around an oscillating airfoil, *Int. J. Num. Meth. Fluids*, **9**, 891–892 (1989)
7 Mehta, U. B. Dynamic stall of an oscillating airfoil, *Unsteady Aerodynamics*, AGARD CP-277, Paper No. 23 (1977)
8 Itty, I. P. *PhD Dissertation*, Department of Mechanical Engineering, University of New Mexico (1991)
9 Owczarek, J. *Fundamentals of Gas Dynamics*, International Book Company, Scranton (1964)
10 Gosman, A. D., Pun, W. M., Runchal, A. K., Spalding, D. B. and Wolfshtein, M. *Heat and Mass Transfer in Recirculating Flows*, Academic Press, New York (1969)
11 Sugavanam, A. and Wu, J. C. Numerical study of separated turbulent flow over airfoils, *AIAA J.*, **20**, 464–470 (1982)
12 Itty, I. P. and Leith, J. R. Vortex growth in the near wake during dynamic stall, *Proc. AIAA Atmos. Flight Mech. Conf.* (1992)
13 Lomax, H. and Mehta, U. B. Some physical and numerical aspects of computing the effects of viscosity on fluid flow, *Computational Methods in Viscous Flows* (Ed. Habashi, W. G.), Vol. 3 (1984)
14 Cebeci, T., Thiele, F., Williams, P. G. and Stewartson, K. On the calculation of symmetric wakes. 1. Two-dimensional flows, *Num. Heat Trans.*, **2**, 35–60 (1979)
15 Michos, A., Bergles, G. and Athanassiadis, N. Aerodynamic characteristics of NACA 0012 Airfoil in relation to wind generators, *Wind Eng.*, **7**, 247–262 (1983)
16 De Ruyck, J. and Hirsch, Ch. Turbulence structures in the wake of an oscillating airfoil, *Unsteady Turbulent Shear Flows* (Eds. Michael, R., Cousteix, J. and Houdeville, R.) Springer-Verlag, New York (1981)
17 Orszag, S. A. and Israeli, M. Numerical simulation of viscous incompressible flows, *A. Rev. Fluid Mech.*, **6**, 281–318 (1974)
18 McAlister, K. W., Carr, L. W. and McCroskey, W. J. Dynamic stall experiments on oscillating airfoil, *NASA TP-1100* (1976)
19 McCroskey, W. J., McAlister, K. and Pucci, S. An experimental study on advanced airfoil sections, NASA TM-84245 (1982)